Optimizing Sintering Temperature for Enhanced Piezoelectric Performance in PMT-PNT-PZT Ceramics

Shaoyang Yuan , Junjun Wang * , Junjun He , Liqiang Liu , Yufang Jiao , Yan Mu , Fengmin Wu *

Posted Date: 28 January 2026

doi: 10.20944/preprints202601.2204.v1

Keywords: PZT-based ceramics; sintering temperature; piezoelectric performance; figure of merit

Article

Optimizing Sintering Temperature for Enhanced Piezoelectric Performance in PMT-PNT-PZT Ceramics

Shaoyang Yuan [1], Junjun Wang [1,2,3,*], Junjun He [2], Liqiang Liu [3], Yufang Jiao [1], Yan Mu [1] and Fengmin Wu [1,*]

[1] School of Science, Harbin University of Science and Technology, Harbin 150080, China

[2] Harbin Kaina Technology Co., Ltd, Harbin 150080, China

[3] Harbin Hatran Navigation Technology Co., Ltd, Harbin 150080, China

* Correspondence: wangjunjun8689@hrbust.edu.cn (J.W.); fmwu@hrbust.edu.cn (F.W.)

Abstract

$0.006Pb(Mn_{1/3}Ta_{2/3})O_3$-$0.114Pb(Ni_{1/3}Ta_{2/3})O_3$-$0.43PbZrO_3$-$0.45PbTiO_3$ lead-based ceramics (PMT-PNT-PZT) were synthesized via the solid-state reaction at different sintering temperatures to study their effects on phase structure, microstructure, and electrical properties. The maximum mechanical quality factor (Q_m) and relative permittivity (ε_r) were achieved at the sintering temperature of 1200 °C. The piezoelectric constant d_{33} of 400 pC/N was obtained at 1180 °C, which is attributed to the high grain density and the significant contribution from the remanent polarization and permittivity product ($P_r\varepsilon_r$ = 39115 μC/cm²). Compared with commercial PZT4 ceramics, the present composition sintered at 1180 °C exhibits an optimal balance between d_{33} and Q_m, together with the superior figure of merit (FOM = 2.04×10^5 pC/N). Furthermore, it demonstrates excellent temperature stability in electromechanical coupling performance.

Keywords: PZT-based ceramics; sintering temperature; piezoelectric performance; figure of merit

1. Introduction

Piezoelectric materials enable efficient interconversion between electrical and mechanical energy, making them essential functional components in transducers, actuators, sensors, and energy harvesters [1–6]. Among them, lead-based ceramics such as PZT have been widely adopted owing to their excellent piezoelectric and electrical properties [7–14]. To further improve piezoelectric performance, lead-based relaxor ceramics have been developed, leveraging their distinctive microstructures to achieve enhanced functional behavior.

PZT-based solid-solution piezoelectric ceramics are often modified or doped for specific applications. The introduction of rare earth elements Sm^{3+} and Eu^{3+} in PMN-PT ceramics has proven effective in improving dielectric properties [15–17]. Similarly, the incorporation of Mn and Fe has been reported to effectively enhance the mechanical quality factor [18–21]. Another strategy involves forming relaxor solid solutions, such as $Pb(Ni_{1/3}Nb_{2/3})O_3$-$PbZrO_3$-$PbTiO_3$ [22], $Pb(Sn_{1/3}Nb_{2/3})O_3$-$Pb(Zn_{1/3}Nb_{2/3})O_3$-$Pb(Zr,TiO_3)$ [23], $Pb(Sc_{1/2}Nb_{1/2})O_3$-$PbTiO_3$ [24] to enhance piezoelectric performance. While many studies on PZT-based ceramics focus on increasing the piezoelectric constant d_{33} or the planar electromechanical coupling factor k_p , only a limited number aim to achieve a balanced improvement in both d_{33} and Q_m. This balance is crucial for high-power applications, as d_{33} influences the sensitivity of ultrasonic transducers, while Q_m is associated with heat generation under high drive conditions [25,26]. Therefore, the coordination of d_{33} and Q_m is of great significance for high-power application materials [27]. In this work, $0.006Pb(Mn_{1/3}Ta_{2/3})O_3$-$0.114Pb(Ni_{1/3}Ta_{2/3})O_3$-$0.43PbZrO_3$-$0.45PbTiO_3$ (PMT-PNT-PZ-PT) is designed to simultaneously enhance d_{33} and Q_m, showing promising potential for high-power device applications.

 doi:10.20944/preprints202601.2204.v1

Sintering temperature plays a critical role in determining the properties of piezoelectric ceramics. MnO_2-doped PZT-PZN ceramics were meticulously prepared at a high temperature of 900℃, exhibiting an impressive d_{33} of 330 pCN^{-1} and a remarkable Q_m of 1000 [28]. The $Pb(Mn_{1/3}Nb_{2/3})O_3$-$Pb(Ni_{1/3}Nb_{2/3})O_3$-$Pb(Zr_{0.50}Ti_{0.50})O_3$ (PMN-PNN-PZT) ceramics were sintered at 900 °C, exhibiting a d_{33} of 346 pCN^{-1} and a Q_m of 1130 [29]. The PMN-PZT-Li_2CO_3 ceramics were sintered at a temperature of 940 °C, exhibiting a high quality factor Q_m (2264), a high Curie temperature T_c (317 °C) and an impressive dielectric constant (1216) [30]. The PSNT-Mn with $LiBiO_2$ ceramics were sintered at 950 °C, resulting in d_{33} = 340 pCN^{-1}, Q_m = 800, T_c = 263 °C [31]. PNN-PZN-PMN-PZ-PT ceramics were sintered at 950 °C, exhibit excellent piezoelectric properties d_{33}^* = 503 pmV^{-1}, Q_m = 471 [32]. By exploring the influence of the sintering temperature (T_s) on the structure of PMT-PNT-PZ-PT ceramic, the best T_s was found to obtain good electrical properties.

In this work, $0.4Pb(Ni_{1/3}Ta_{2/3})O_3$-$0.6PbTiO_3$ exhibits a high dielectric property, and it induces lead vacancies by incorporating Ni^{2+} and Ta^{5+} into the B site of PZT, facilitating domain switching and effectively enhancing the piezoelectric performance of the ceramic, $0.006Pb(Mn_{1/3}Ta_{2/3})O_3$-$0.114Pb(Ni_{1/3}Ta_{2/3})O_3$-$0.43PbZrO_3$-$0.45PbTiO_3$ (PMT-PNT -PZ-PT) is designed to simultaneously enhance d_{33} and Q_m, showing promising potential for high-power device applications.

2. Materials and Methods

$0.006Pb(Mn_{1/3}Ta_{2/3})O_3$-$0.114Pb(Ni_{1/3}Ta_{2/3})O_3$-$0.43PbZrO_3$-$0.45PbTiO_3$ (abbreviated as PMT-PNT-PZ-PT) ceramics were fabricated via the conventional solid-state method. PbO (99.9%), ZrO_2 (99.99%), NiO(99%), Ta_2O_5 (99.99%) and MnO_2 (99%) were used as the starting materials. All the starting materials were weighed based on the stoichiometric ratio and then milled in the alcohol with zirconia balls for 12 h. The resulting mixture was dried and pre-burned at 750 °C for 2.5 h, and the calcined powder was ball-milled for 24 h again. The powder was mixed with 7 wt.% polyvinyl alcohol (PVA) as a binder, which provides cohesion and green strength for shaping. The mixture was then uniaxially pressed into gray disks with a diameter of 13 mm. Subsequently, the prepared disks underwent a debinding process at 550 °C to completely remove the PVA. Finally, the disks were embedded in a sacrificial powder with the same composition as the ceramic matrix to prevent reaction and deformation, followed by sintering for 2.5 hours at different temperatures (T_s = 1180, 1200, 1250, and 1270 °C). To facilitate electrical properties characterization, the samples were polished and coated with silver to serve as electrodes.

The crystalline phases of the ceramics were evidenced by XRD (D/max-rB 12kW X-ray diffractometer). The fractured surface micromorphology of the sintered samples was determined by the scanning electron microscopy (SEM, SU5000). The temperature dependence of dielectric constant and loss were measured using a LCR test instrument (Agilent, E4980A, Santa Clara, CA, USA) from the room temperature to 450 ℃ at 0.1 kHz, 1 kHz, 10 kHz, 100 kHz, 1 MHz. For piezoelectric properties, the ceramics were poled in a silicone oil bath at 150 °C under a DC field of 3 kV/mm for 15 minutes. Poling at this elevated temperature lowers the coercive field, thereby facilitating domain alignment under the applied electric field. The piezoelectric coefficient d_{33} was measured by a quasi-static meter (ZJ-4A). The ferroelectric hysteresis loops of the ceramic samples were measured by the ferroelectric test system. (premier II, Radiant Tech, Albuquerque, USA). The mechanical quality factor (Q_m) and electromechanical coupling factor (k_p) were calculated based on the IEEE standards using the Agilent 4294A Precision Impedance Analyzer, as follows:

$$Q_m = \frac{1}{4\pi(f_a - f_r)R_1(C_0 + C_1)} \quad (1)$$

$$\frac{1}{k_p^2} = 0.395 \times \frac{f_r}{f_a - f_r} + 0.574 \quad (2)$$

 doi:10.20944/preprints202601.2204.v1

3. Results and Discussion

Figure 1 presents the XRD patterns of PMT-PNT-PZ-PT ceramics sintered at different temperatures (1180 °C, 1200 °C, 1250 °C, and 1270 °C). It can be seen that the positions of the most intense diffraction peaks remain consistent across all sintering temperatures, with all samples exhibiting characteristic peaks of a perovskite structure. This indicates that the doped ions have been successfully incorporated into the perovskite lattice, forming a stable solid solution. The crystal structure is identified as tetragonal for the PMT-PNT-PZ-PT ceramics, as evidenced by a (200)/(002) peak intensity ratio of approximately 1:2. Furthermore, the intensity of the (110) diffraction peak varies with sintering temperature, suggesting that the sintering process influences the crystallinity of the ceramics.

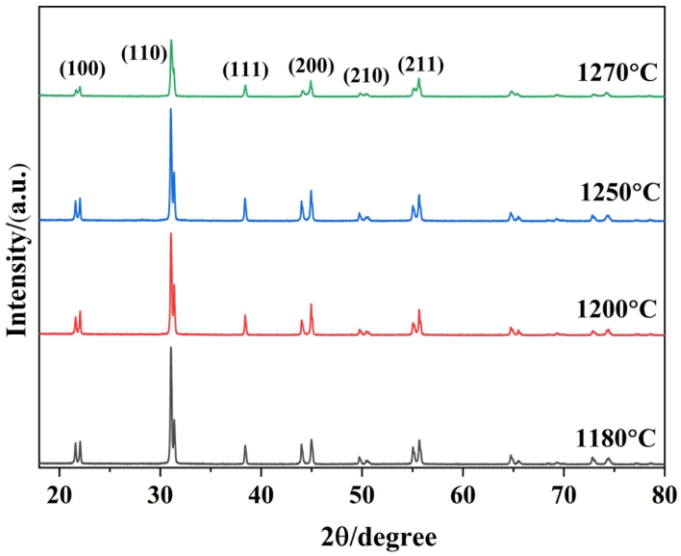

Figure 1. XRD pattern of PMT-PNT-PZ-PT ceramics at different sintering temperatures.

Figure 2 (a–d) displays the SEM micrographs of PMT-PNT-PZ-PT ceramics sintered at different temperatures. The samples sintered at 1180 °C and 1200 °C exhibit a dense microstructure, well-developed grains, and no visible pores or abnormal grain growth, suggesting excellent ceramic quality and optimal electrical properties at these temperatures. The grain size as a function of sintering temperature is summarized in Figure 2 (e and f). As the sintering temperature increases, the average grain size shows a clear upward trend, indicating that higher temperatures promote grain growth. However, the emergence of pores at elevated temperatures likely reduces the densification of the ceramics, thereby degrading their electrical performance. In the sample sintered at 1270 °C, the grains are closely bonded and exhibit a tendency to coalesce, which can be attributed to the partial melting of over-sintered grains.

 doi:10.20944/preprints202601.2204.v1

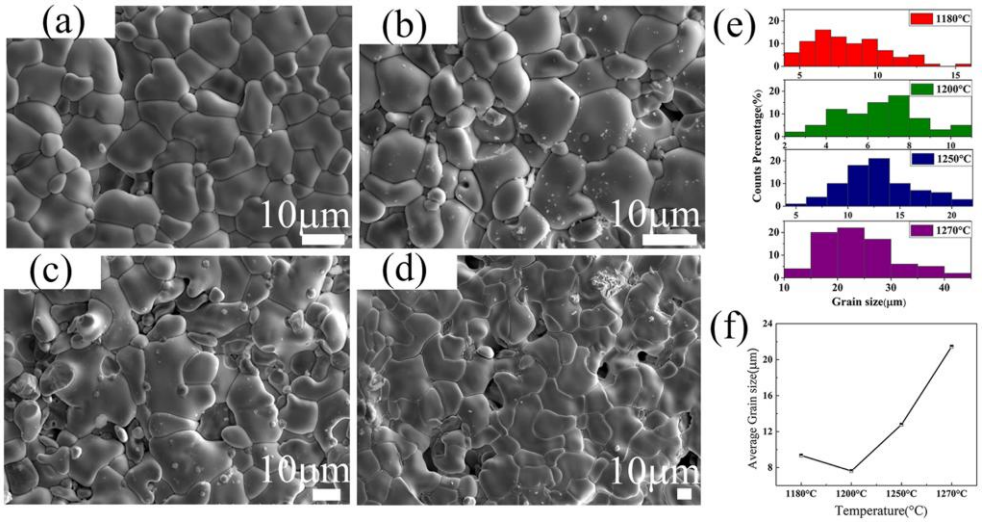

Figure 2. SEM microstructure of calcined ceramic at different sintering temperature (a)1180 °C, (b)1200 °C, (c)1250 °C, (d)1270 °C, (e)Grain size distribution, (f) variations of average grain size.

Figure 3(a-d) illustrates the temperature dependence of the dielectric constant and loss for PMT-PNT-PZ-PT ceramics measured from room temperature to 450 °C at frequencies of 0.1 kHz, 1 kHz, 10 kHz, 100 kHz, 1MHz. A single permittivity peak is observed near the Curie temperature (approximately 300 °C) for all compositions, indicating a ferroelectric–paraelectric phase transition. At room temperature, the ceramics exhibit a purely tetragonal phase, which is consistent with the XRD analysis. As frequency increases, the loss (*tanδ*) values gradually decrease due to polaron relaxation processes associated with localized oxygen vacancies present in the crystal lattice [33]. At the low frequency, *tanδ* start to rapidly increase beyond T_c due to thermally-activated space charge conduction behavior [34].

To further analyze the dielectric behavior, a modified empirical formula was employed to evaluate the dielectric dispersion and diffusivity (γ) of the phase transition. The calculation of γ based on the Curie-Weiss law can be formulated as follows

$$1/\varepsilon - 1/\varepsilon_m = (T - T_m)^{\gamma}/C \tag{3}$$

where ε_m is the maximum dielectric constant at T_m. Figure 3(e) further reveals that all samples exhibit characteristic relaxor ferroelectric behavior with a diffuse phase transition, regardless of sintering temperature. As the sintering temperature increases, the diffuseness parameter γ gradually decreases, suggesting that grain growth tends to suppress the relaxor characteristics. Notably, in the sample sintered at 1180 °C, the dielectric loss (*tanδ*) remains below 0.02 at 10 kHz. This low loss profile is highly favorable for applications such as ultrasonic transducers.

The *P-E* loops of PMT-PNT-PZ-PT measured at room temperature are shown in Figure 4. With the increase of sintering temperature, *P-E* loops become asymmetrical gradually. The presence of acceptor-oxygen vacancy defect dipoles leads to the generation of an internal bias field [35–37]. The internal bias field can be calculated by

$$E_i = \frac{\left|E_c^+\right| - \left|E_c^-\right|}{2} \tag{4}$$

Figure 4(b) shows the changing rule of E_c^+, $\left|E_c^-\right|$ and E_i as a function of sintering temperature. The E_i increases proportionally with the sintering temperature, whereby higher temperatures lead to elevated concentrations of oxygen vacancies and defect dipoles, ultimately resulting in an augmented internal bias field.

 doi:10.20944/preprints202601.2204.v1

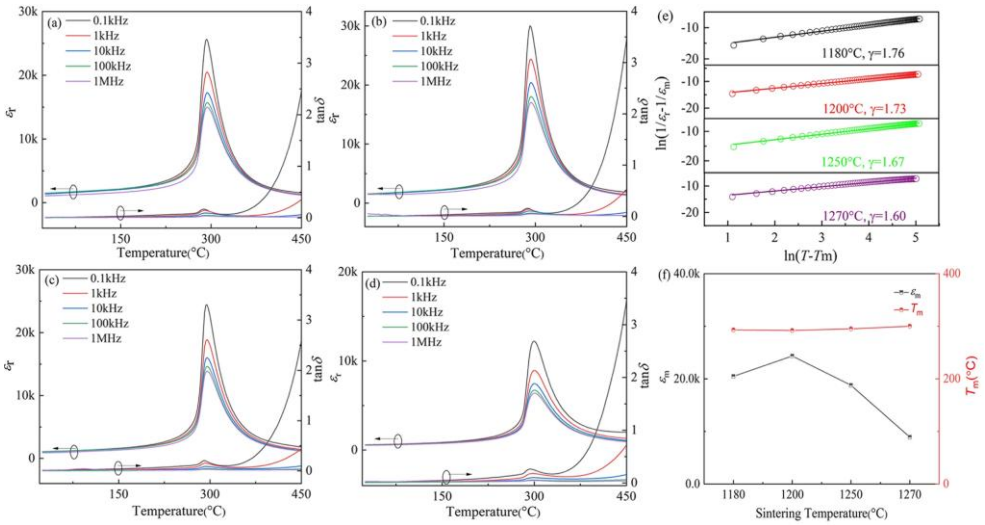

Figure 3. Temperature dependence of dielectric constant and dielectric loss of PMT-PNT-PZ-PT ceramics with different frequencies at different sintering temperature: (a)1180 °C, (b)1200 °C, (c)1250 °C, (d)1270 °C, (e)Modified Curie-Weiss fitting curves of PMT-PNT-PZ-PT ceramics sintered at different temperatures, (f)Variations of ε_m, T_m..

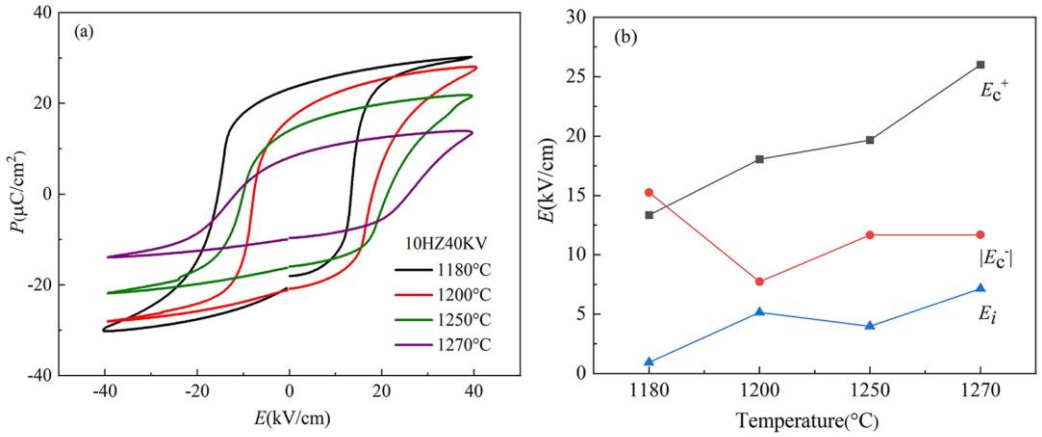

Figure 4. Ferroelectric properties of PMT-PNT-PZ-PT ceramics: (a) *P-E* hysteresis loops, (b)The coercive field of positive electric field (E_c^+), negative electric field(E_c^-), and the internal bias field (E_i).

Figure 5 describes the relationship between d_{33}, Q_m and sintering temperature. The d_{33} value gradually decreases with the sintering temperature, while the Q_m value initially increases and then subsequently decreases. In order to assess the optimal comprehensive properties of PMT-PNT-PZ-PT ceramics, figure of merit (FOM) is defined as FOM = $d_{33} \times Q_m$ [38,39]. According to Figure 5, the optimum-integrated performances of d_{33} (400 pC/N), Q_m (509), and FOM (203600 pC/N) for the sintering temperature 1180 °C. The observed trends can be explained by the incorporation of Mn ions and the associated generation of oxygen vacancies for charge compensation. These point defects act as pinning centers for domain walls, restricting their motion [40,41]. This pinning effect is responsible for the gradual decrease in d_{33} and the initial increase in Q_m with sintering temperature, as domain wall contributions to dielectric and piezoelectric responses are reduced while mechanical losses are minimized. For perovskite ferroelectrics, the piezoelectric coefficient d_{33} can be expressed as [42]:

$$d_{33} = 2P_r Q \varepsilon_0 \varepsilon_r \quad (5)$$

where P_r is residual polarization, ε_r is the dielectric constant, ε_0 is the dielectric constant in vacuum, Q is the electrostrictive coefficient (for the same material Q is the same). When the sintering

 doi:10.20944/preprints202601.2204.v1

temperature is 1180 °C, the ceramics have the largest piezoelectric constant (d_{33}). Combined with Figure 5 (b), the variation of d_{33} and $P_r\varepsilon_r$ is consistent, so the large d_{33} comes from $P_r\varepsilon_r$. The analysis shows that the Mn enters the lattice at higher temperatures. To uphold the electrical neutrality of the cell, a greater number of oxygen vacancies are generated within the material. The existence of oxygen vacancies hinders the mobility of the domain wall, resulting in a decrease in d_{33} and k_p, while Q_m exhibits an increase. Incorporation of Mn ions into the system induces ceramic "strengthening" effects, leading to an enhancement in Q_m.

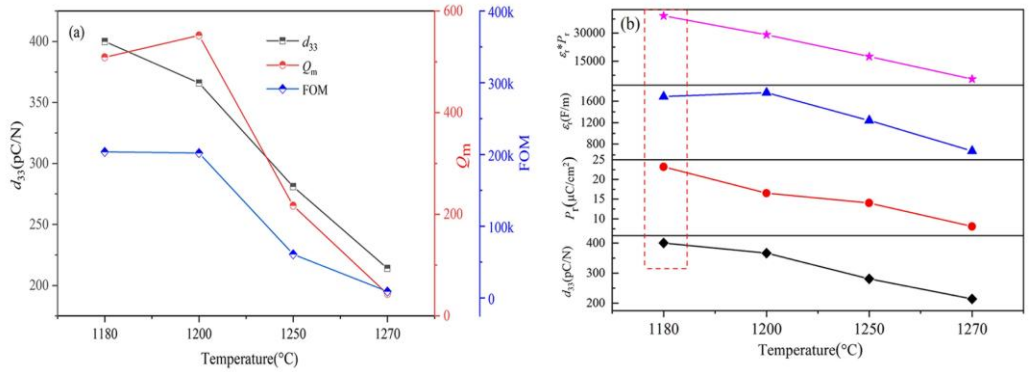

Figure 5. (a)Values of Q_m, d_{33} and FOM with the sintering temperatures, (b)The electrical properties of PMT-PNT-PZ-PT ceramics sintered at different temperatures.

The properties of the ceramics are compared with those of commercial PZT4 ceramics and other ceramics, as presented in Table 1. We effectively reconcile the trade-off between d_{33} and Q_m, thereby presenting a novel approach to enhance the sensitivity of ultrasonic transducers while minimizing heat generation. Furthermore, it reveals significant advantages in various other properties compared to the aforementioned piezoelectric ceramics.

Table 1. Comparison of electrical properties between the present PMT-PNT-PZ-PT ceramic (sintered at 1180°C) and other representative piezoelectric ceramics.

Material	ε_r	k_p	k_t	T_c(℃)	d_{33}(pC/N)	Q_m	FOM(pC/N)	Ref
PMT-PNT-PZ-PT(1180 °C)	1686	0.65		304	400	509	2.04×10^5	This work
PZT4	1300	0.58		328	289	500	1.50×10^5	43
PMN-PZT				216	1530	100	1.53×10^5	44
BS–yPT–xBMS	1384	0.50		410	330	84	2.80×10^4	45
KNNS-BNZ-xBZ	3460	0.58	0.45		610	34	2.10×10^4	46

4. Conclusions

The effects of sintering temperature on the phase structure and electrical properties of $0.006Pb(Mn_{1/3}Ta_{2/3})O_3$-$0.114Pb(Ni_{1/3}Ta_{2/3})O_3$-$0.43PbZrO_3$-$0.45PbTiO_3$ (PMT-PNT-PZ-PT) ceramics are comprehensively investigated. The sintering temperature plays a critical role in tailoring the microstructure and electrical performance of PMT-PNT-PZ-PT ceramics. The ceramic sintered at 1200 °C exhibits the smallest grain size along with the highest mechanical quality factor (Q_m) and relative permittivity (ε_r). The piezoelectric constant d_{33} (400 pC/N) is achieved at 1180 °C, accompanied by a significant $P_r\varepsilon_r$ (39115 μCcm^{-2}). Compared to commercial PZT-4 ceramics, the composition sintered at 1180 °C attained an optimal balance between d_{33} and Q_m, resulting in a superior comprehensive figure of merit (FOM = 2.04×10^5 pC/N). These results not only provide a viable candidate material for high-power and temperature-stable piezoelectric devices but also offer valuable insights into the processing-property relationships in complex perovskite ceramics.

 doi:10.20944/preprints202601.2204.v1

Author Contributions: Conceptualization, Junjun Wang; Data curation, Shaoyang Yuan and Yan Mu; Formal analysis, Shaoyang Yuan, Liqiang Liu, Yufang Jiao and Yan Mu; Software, Yufang Jiao, Junjun He and Yan Mu; Writing – original draft, Shaoyang Yuan, Junjun Wang, Yufang Jiao and Yan Mu; Writing – review & editing, Junjun Wang and Fengmin Wu. All authors have read and agreed to the published version of the manuscript.

Funding: This study is supported by the Heilongjiang Provincial Natural Science Foundation of China (No. PL2024A005).

Data Availability Statement: The original contributions presented in the study are included in the article, further inquiries can be directed to the corresponding authors.

Acknowledgments: This study is supported by the Heilongjiang Provincial Natural Science Foundation of China (No. PL2024A005).

Conflicts of Interest: The authors declare no conflict of interest.

References

1. X. R. Yang, W. L. Li, Y. L. Qiao, et al. High Energy-Storage Density of Lead-Free $(Sr_{1-1.5x}Bi_x)Ti_{0.99}Mn_{0.01}O_3$ Thin Films Induced by Bi^{3+}-VSr Dipolar Defects. Phys. Chem. Chem. Phys. **2019**, 21(29), 16359-16366.
2. G. Clementi, G. Lombardi, S. Margueron, et al. $LiNbO_3$ films-A low-cost alternative lead-free piezoelectric material for vibrational energy harvesters. Mech. Syst. Signal Pr. **2020**, 149, 107171.
3. E. Brusa, A. Carrera, C. Delprete. A Review of Piezoelectric Energy Harvesting: Materials, Design, and Readout Circuits. Actuators. 2023, 12(12), 457.
4. Y. Yan, J. E. Zhou, D. Maurya, et al. Giant Piezoelectric Voltage Coefficient in Grain-Oriented Modified $PbTiO_3$ Material. Nat. Commun. **2016**, 7(1), 13089.
5. J. F. Tressler, S. Alkoy, R. E. Newnham. Piezoelectric Sensors and Sensor Materials. J. Electroceram. **1998**, 2(4), 257-272.
6. X. Yang, W. Li, Y. Zhang, et al. High Energy Storage Density Achieved in Bi^{3+}-Li^+ Co-Doped $SrTi_{0.99}Mn_{0.01}O_3$ Thin Film via Ionic Pair Dooping-Engineering. J. Eur. Ceram. Soc. **2020**, 40(3), 706-711.
7. A. Bartasyte, G. Clementi, Q. Micard, et al. Material strategies to enhance the performance of piezoelectric energy harvesters based on lead-free materials. J. Micromech. Microeng. 2023, 33(5), 053001.
8. L. Yang, H. Huang, Z. Xi, et al. Simultaneously Achieving Giant Piezoelectricity and Record Coercive Field Enhancement in Relaxor-Based Ferroelectric Crystals. Nat. Commun. **2022**, 13(1), 2444.
9. H. Wu, S. Fu, S. Wang, et al. Electrical Current Visualization Sensor Based on Magneto-Electrochromic Effect. Nano Energy **2022**, 98, 107226.
10. Y. Zhang, W. Jie, P. Chen, et al. Ferroelectric and Piezoelectric Effects on the Optical Process in Advanced Materials and Devices. Adv. Mater. **2018**, 30(34), 1707007.
11. Y. Wang, S. Wang, Y. Meng, et al. Pyro-Catalysis for Tooth Whitening via Oral Temperature Fluctuation. Nat. Commun. **2022**, 13(1), 4419.
12. Z. Li, X. Yi, J. Yang, et al. Designing Artificial Vibration Modes of Piezoelectric Devices Using Programmable, 3D Ordered Structure with Piezoceramic Strain Units. Adv. Mater. **2022**, 34(2), 2107236.
13. Q. Li, G. Dong, Y. Zhao, et al. High piezoelectric properties and excellent thermal stability in PNN-modified lead zirconate titanate piezoceramics. J. Am. Ceram. Soc. **2025**, 108(9), 20643.
14. D. Li, X. Zeng, Z. Li, et al. Progress and Perspectives in Dielectric Energy Storage Ceramics. J. Adv. Ceram. **2021**, 10(4), 675-703.
15. F. Li, D. Lin, Z. Chen, et al. Ultrahigh Piezoelectricity in Ferroelectric Ceramics by Design. Nat. Mater. **2018**, 17(4), 349-354.
16. R. Yimnirun, S. Ananta, P. Laoratanakul. Dielectric and Ferroelectric Properties of Lead Magnesium Niobate-Lead Zirconate Titanate Ceramics Prepared by Mixed-Oxide Method. J. Eur. Ceram. Soc. **2005**, 25(13), 3235-3242.
17. H. Wang, F. Zhang, Y. Chen, et al. Giant Piezoelectric Coefficient of PNN-PZT-Based Relaxor Piezoelectric Ceramics by Constructing an RT MPB. Ceram. Int. **2021**, 47(9), 12284-12291.

 doi:10.20944/preprints202601.2204.v1

18. C. He, X. Li, Z. Wang, et al. Growth of $Pb(Fe_{1/2}Nb_{1/2})O_3$-$Pb(Yb_{1/2}Nb_{1/2})O_3$-$PbTiO_3$ Piezo-/Ferroelectric Crystals for High Power and High Temperature Applications. Cryst. Eng. Comm **2012**, 14(13), 4407-4413.
19. S. Zhang, S. Lee, D. Kim, et al. Characterization of Mn-Modified $Pb(Mg_{1/3}Nb_{2/3})O_3$-$PbZrO_3$-$PbTiO_3$ Single Crystals for High Power Broad Bandwidth Transducers. Appl. Phys. Lett. **2008**, 93(12), 122908.
20. Z. Xia, Q. Li. Structural Phase Transformation and Electrical Properties of (0.90-x)$Pb(Mg_{1/3}Nb_{2/3})O_3$-x$PbTiO_3$ -0.10$Pb(Fe_{1/2}Nb_{1/2})O_3$ Ferroelectric Ceramics Near the Morphotropic Phase Boundary. Acta Mater. **2007**, 55(18), 6176-6181.
21. Y. Hou, M. Zhu, F. Gao, et al. Effect of MnO_2 Addition on the Structure and Electrical Properties of $Pb(Zn_{1/3}Nb_{2/3})0.20(Zr_{0.50}Ti_{0.50})0.80O_3$ Ceramics. J. Am. Ceram. Soc. **2004**, 87(5), 847-850.
22. X. Gao, J. Wu, Y. Yu, et al. Giant Piezoelectric Coefficients in Relaxor Piezoelectric Ceramic PNN-PZT for Vibration Energy Harvesting. Adv. Funct. Mater. **2018**, 28(30), 1706895.
23. S. Zhao, H. Wu, Q. Sun. Study on PSN-PZN-PZT Quaternary Piezoelectric Ceramics Near the Morphotropic Phase Boundary. Mater. Sci. Eng. B **2005**, 123(3), 203-210.
24. Z. Wang, X. Li, C. He, et al. Characteristic Electrical Properties of $Pb(Sc_{1/2}Nb_{1/2})O_3$-$PbTiO_3$ Ferroelectric Crystals. J. Mater. Sci. **2015**, 50(11), 3970-3975.
25. T. Huang, J. Fu, R. Zuo. A $Pb(Zr,Ti)O_3$-$Pb(Zn_{1/3}Nb_{2/3})O_3$-$Bi(Mn_{2/3}Sb_{1/3})O_3$ Quaternary Solid Solution Ceramic with Low Sintering Temperature, High Piezoelectric Coefficient and Large Mechanical Quality Factor. J. Mater. Sci.: Mater. Electron. **2019**, 30(10), 9540-9546.
26. H. Zhang, J. Shen, J. Tian, et al. Elastic, Dielectric and Piezoelectric Properties of Fe_2O_3 Doped PMnS-PZN-PZT Ceramics. Ferroelectrics **2016**, 491(1), 15-26.
27. H. J. Lee, S. Zhang. Design of Low-Loss 1-3 Piezoelectric Composites for High-Power Transducer Applications. IEEE Trans. Ultrason. Ferroelectr. Freq. Control **2012**, 59(9), 1969-1975.
28. S. M. Lee, S. H. Lee, C. B. Yoon, et al. Low-Temperature Sintering of MnO_2-Doped PZT-PZN Piezoelectric Ceramics. J. Electroceram. **2007**, 18(3), 311-315.
29. S. Dabas, M. Kumar, P. Chaudhary, et al. Enhanced Magneto-Electric Coupling and Energy Storage Analysis in Mn-Modified Lead Free $BiFeO_3$-$BaTiO_3$ Solid Solutions. J. Appl. Phys. **2019**, 126(13), 134102.
30. J. Yoo, C. Lee, Y. Jeong, et al. Microstructural and Piezoelectric Properties of Low Temperature Sintering PMN-PZT Ceramics with the Amount of Li_2CO_3 Addition. Mater. Chem. Phys. **2005**, 90(2-3), 386-390.
31. S. Zhang, R. Xia, T. R. Shrout. Low Temperature Sintering and Properties of Piezoelectric Ceramics PSNT-Mn with $LiBiO_2$ Addition. Mater. Sci. Eng. B **2006**, 129(1-3), 131-134.
32. C. K. I. Tan, M. Sharifzadeh Mirshekarloo, S. C. Lai, et al. PNN-PZN-PMN-PZ-PT Multilayer Piezoelectric Ceramic with Low Sintering Temperature. Int. J. Appl. Ceram. Technol. **2016**, 13(5), 889-895.
33. Z. Li, H. Fan. Polaron Relaxation Associated with the Localized Oxygen Vacancies in $Ba_{0.85}Sr_{0.15}TiO_3$ Ceramics at High Temperatures. J. Appl. Phys. **2009**, 106(5), 054102.
34. Y. Chen, L. Li, Z. Zhou, et al. La_2O_3-Modified $BiYbO_3$-$Pb(Zr,Ti)O_3$ Ternary Piezoelectric Ceramics with Enhanced Electrical Properties and Thermal Depolarization Temperature. J. Adv. Ceram. **2023**, 12(8), 1593-1611.
35. S. Zhang, L. Lebrun, C. A. Randall, et al. Growth and Electrical Properties of (Mn, F) Co-Doped 0.92$Pb(Zn_{1/3}Nb_{2/3})O_3$ -0.08$PbTiO_3$ Single Crystal. J. Cryst. Growth **2004**, 267(1-2), 204-212.
36. X. Chen, Y. Liao, H. Wang, et al. Phase Structure and Electric Properties of $Bi_{0.5}(Na_{0.825}K_{0.175})_{0.5}TiO_3$ Ceramics Prepared by a Sol-Gel Method. J. Alloys Compd. **2010**, 493(1-2), 368-371.
37. A. Chauhan, S. Patel, R. Vaish. Mechanical Confinement for Improved Energy Storage Density in BNT-BT-KNN Lead-Free Ceramic Capacitors. AIP Adv. **2014**, 4(8), 087106.
38. S. W. Kim, H. C. Lee. Development of PZN-PMN-PZT Piezoelectric Ceramics with High d_{33} and Q_m Values. Materials **2022**, 15(20), 7070.
39. Y. Yang, E. Sun, Z. Xu, et al. Sm and Mn co-doped PMN-PT piezoelectric ceramics: Defect engineering strategy to achieve large d_{33} and high Q_m. J. Mater. Sci. Technol. 2023, 137, 143-151.
40. B. Kamboj, V. Tanwar, A. Yadav, et al. Site-Specific Selenium Substitution Enhances Charge Storage Performance in Solid-State Flexible $MnFe_2O_4$-Based Supercapacitor Devices via Modulated d-States. Adv. Funct. Mater. 2025, 16045.

 doi:10.20944/preprints202601.2204.v1

41. Y. Wu, Y. Cheng, S. Guan, et al. KNN-Based Lead-Free Piezoelectric Ceramics with High Q_m and Enhanced d_{33} via a Donor-Acceptor Codoping Strategy. Inorg. Chem. **2023**, 62(37), 15094-15103.
42. L. Bian, K. Zhu, Q. Wang, et al. Performance Enhancement of Ultrasonic Transducer Made of Textured PNN-PZT Ceramic. J. Adv. Dielectr. **2022**, 12(04), 2244003.
43. G. H. Haertling. Ferroelectric Ceramics: History and Technology. J. Am. Ceram. Soc. **1999**, 82(4), 797-818.
44. S. Zhang, S. M. Lee, D. H. Kim, et al. Temperature Dependence of the Dielectric, Piezoelectric, and Elastic Constants for $Pb(Mg_{1/3}Nb_{2/3})O_3$-$PbZrO_3$-$PbTiO_3$ Piezocrystals. J. Appl. Phys. **2007**, 102(11), 114103.
45. Y. Feng, C. Yang, X. Guo, et al. Achieving Both Large Piezoelectric Constant and Low Dielectric Loss in $BiScO_3$-$PbTiO_3$–$Bi(Mn_{2/3}Sb_{1/3})O_3$ High-Temperature Piezoelectric Ceramics. J. Adv. Dielectr. **2022**, 12(06), 2250017.
46. C. Zhou, J. Zhang, W. Yao, et al. Remarkably Strong Piezoelectricity, Rhombohedral-Orthorhombic-Tetragonal Phase Coexistence and Domain Structure of $(K,Na)(Nb,Sb)O_3$-$(Bi,Na)ZrO_3$-$BaZrO_3$ Ceramics. J. Alloys Compd. **2020**, 820, 153411.